Am J Transl Res 2026;18(1):676-690
www.ajtr.org /ISSN:1943-8141/AJTR0168276

Original Article

Multimodal optical coherence tomography and angiography and serologic markers for accurate early diagnosis of dysthyroid optic neuropathy

Yusheng Zhao[1,2], Qian Xiao[3], Bin Fan[1], Lu Tang[3], Xiaohu Chen[4], Yan Dai[1]

[1]Department of Ophthalmology, The Affiliated Hospital of Southwest Medical University, Luzhou 646000, Sichuan, China; [2]Yanting Tumor Hospital, Mianyang 621600, Sichuan, China; [3]Department of Ophthalmology, Affiliated Hospital of North Sichuan Medical College, Nanchong 646000, Sichuan, China; [4]Department of Ophthalmology, Mianyang Central Hospital, Mianyang 621000, Sichuan, China

Received August 22, 2025; Accepted November 25, 2025; Epub January 15, 2026; Published January 30, 2026

Abstract: Objective: To assess the value of optical coherence tomography (OCT) and OCT angiography (OCTA) for the early diagnosis of dysthyroid optic neuropathy (DON) in patients with thyroid-associated orbitopathy (TAO). Methods: This retrospective study (2022-2024) included 52 TAO eyes (22 DON, 30 non-DON) and 52 healthy controls. OCT/OCTA scans evaluated structural features (ganglion cell complex, peripapillary retinal nerve fiber layer, Bruch's membrane opening-minimum rim width [BMO-MRW]) and vascular features (superficial retinal capillary plexus [SRCP] density, choroidal capillary vascular density, foveal avascular zone [FAZ] area). Contrast sensitivity function (CSF), thyroid peroxidase antibody (TPOAb) status, and glutamate levels were also analyzed. Multivariate logistic regression identified risk factors, and receiver operating characteristic curves evaluated diagnostic performance. Results: Most structural OCT features showed no significant differences, except CSF, which was significantly reduced in DON eyes ($P < 0.001$). Vascular features such as SRCP density and choroidal capillary density decreased progressively in DON, while FAZ area was significantly larger (all $P < 0.001$). TPOAb positivity and glutamate levels were highest in the DON group ($P < 0.001$). Multivariate analysis identified SRCP density, FAZ area, TPOAb positivity, and glutamate concentration as independent risk factors for DON. A combined model of BMO-MRW and subfoveal choroidal thickness achieved the highest diagnostic accuracy (AUC = 0.940, sensitivity = 88.0%, specificity = 90.0%). Conclusions: Multimodal imaging combining OCT and OCTA features improves the sensitivity and specificity of early DON diagnosis, offering a reliable, noninvasive screening approach for clinical practice.

Keywords: Thyroid-associated orbitopathy, dysthyroid optic neuropathy, optical coherence tomography, optical coherence tomography angiography, multimodal imaging

Introduction

Thyroid-associated orbitopathy (TAO), an autoimmune inflammatory disorder commonly associated with Graves' disease, affects approximately 25-50% of hyperthyroid patients and can lead to severe ocular complications [1]. Among these, dysthyroid optic neuropathy (DON) represents the most vision-threatening manifestation, occurring in 3-7% of TAO cases [2]. DON results from mechanical compression and ischemic injury to the optic nerve due to enlarged extraocular muscles and orbital fat within the confined bony orbit, possibly causing irreversible visual field defects, color vision loss, or even blindness if not promptly recognized and treated [3]. Despite its severity, early diagnosis remains challenging because conventional clinical signs - such as reduced visual acuity or afferent pupillary defect - often appear only after significant neural damage has occurred [4].

Current diagnostic criteria for DON rely heavily on morphologic assessments, including Hertel exophthalmometry, orbital computed tomography (CT), and magnetic resonance imaging (MRI), to evaluate extraocular muscle enlargement and optic nerve compression [5]. However, these modalities lack sensitivity to detect early microstructural and microvascular alterations in retina and choroid that precede overt struc-

https://doi.org/10.62347/SDKT8956

tural compression [6]. Moreover, up to 30% of DON cases are "clinically silent" at initial presentation, further underscoring the urgent need for objective, non-invasive biomarkers capable of identifying subclinical optic nerve dysfunction [1, 7-9].

In recent years, optical coherence tomography (OCT) and optical coherence tomography angiography (OCTA) have emerged as powerful tools for quantifying retinal and choroidal microstructure and perfusion *in vivo* [10-13]. Studies have reported the thinning of the ganglion cell complex (GCC) and reduced peripapillary retinal nerve fiber layer (pRNFL) thickness in TAO patients, suggesting early neuronal loss [14]. Similarly, OCTA has revealed decreased superficial retinal capillary plexus (SRCP) density and altered foveal avascular zone (FAZ) morphology, implicating microcirculatory insufficiency in DON pathogenesis [15]. Nevertheless, most existing studies focus on isolated features and fail to integrate structural, vascular, functional, and serological data into a unified diagnostic framework [3, 4, 16, 17]. Furthermore, the diagnostic performance of single OCT/OCTA metrics remains suboptimal due to interindividual variability and disease heterogeneity [18, 19].

Despite advances in orbital imaging, the diagnosis of early or subclinical DON remains a major clinical dilemma. Traditional diagnostic criteria - such as optic disc swelling, relative afferent pupillary defect, or visual field loss - are often late manifestations and lack sensitivity in the initial stages of optic nerve compromise. While orbital CT and MRI can visualize extraocular muscle enlargement and optic nerve compression, they are unable to detect microstructural or microvascular alterations in retina and choroid that may precede overt mechanical damage. Moreover, up to one-third of DON cases present without classic signs, leading to delayed intervention and poorer visual outcomes [9].

In this context, non-invasive retinal and choroidal imaging modalities, particularly OCT and OCTA, have emerged as promising tools for detecting early neural and vascular dysfunction in TAO. Recent studies have reported the thinning of GCC, reduced pRNFL thickness, and impaired macular microvasculature in TAO patients, even before the onset of visual symptoms. However, no consensus exists on which features are most predictive of DON, and single-modality assessments often lack sufficient diagnostic accuracy. Therefore, integrating multimodal structural, vascular, and biochemical biomarkers may offer a more comprehensive and sensitive approach for early identification of DON.

This retrospective study pioneers a multimodal diagnostic strategy that combines OCT/OCTA-derived structural and hemodynamic features (e.g., Bruch's membrane opening-minimum rim width [BMO-MRW], subfoveal choroidal thickness [SFCT], SRCP density, FAZ area) with functional metrics (contrast sensitivity function [CSF]) and serological biomarkers (thyroid peroxidase antibody [TPOAb] status, glutamate concentration). We hypothesize that such an integrative approach can significantly enhance the early detection of DON in TAO patients. By validating this model in a well-characterized clinical cohort, our study not only advances the understanding of DON pathophysiology but also provides a clinically translatable, non-invasive screening tool with high sensitivity and specificity. This may enable timely intervention before irreversible vision loss occurs.

Materials and methods

Patient selection

This retrospective cohort study included patients diagnosed with TAO who were evaluated at the Department of Ophthalmology, Mianyang Central Hospital between January 2022 and December 2024. The study was approved by the Ethics Committee of Mianyang Central Hospital, and the requirement for informed consent was waived due to the retrospective nature of the study, in accordance with the Declaration of Helsinki (2013).

Potential cases were identified through electronic medical record search using International Classification of Diseases, 10th Revision coding system for Graves' ophthalmopathy (H06.2) and optic neuropathy (H46.0-H46.9). Eligible patients were required to have: (1) a confirmed diagnosis of TAO based on the criteria proposed by Bartley et al. [20]; (2) the diagnosis of DON defined by the presence of at least two of the following (in the absence of other causes): reduced visual acuity, impaired color vision, visual field defects, relative afferent pupillary defect, or abnormal pattern visual evoked potentials; (3) complete clinical, imaging, and

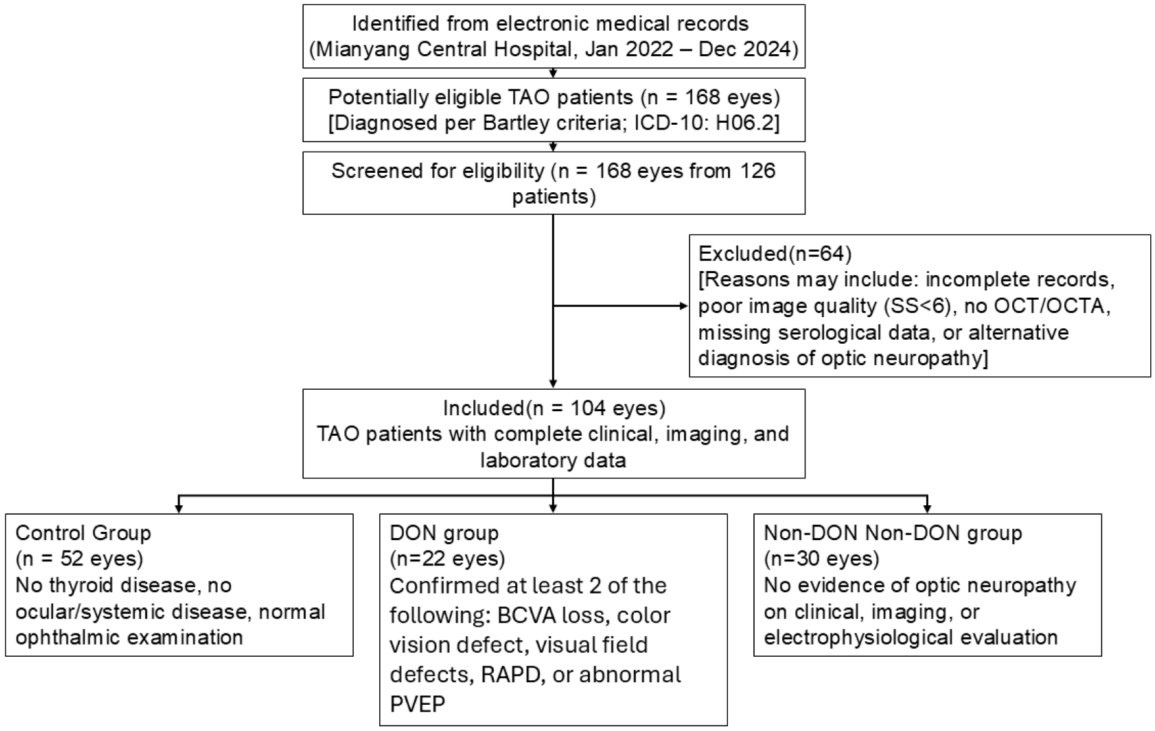

Figure 1. Flow chart of patient selection. Note: Eyes were identified by electronic medical record search using ICD-10 code H06.2. Inclusion required complete clinical documentation, high-quality OCT/OCTA (signal strength ≥ 6), and available serum biomarker data. DON was diagnosed based on the presence of at least two objective signs of optic nerve dysfunction, after exclusion of other causes. Abbreviations: TAO: Thyroid-Associated Orbitopathy; ICD-10: International Classification of Diseases, 10th Revision; SS: Signal Strength; DON: Dysthyroid Optic Neuropathy; BCVA: Best-Corrected Visual Acuity; RAPD: Relative Afferent Pupillary Defect; PVEP: Pattern Visual Evoked Potentials; OCT: Optical Coherence Tomography; OCTA: Optical Coherence Tomography Angiography.

laboratory records; and (4) high-quality OCT/OCTA scans (signal strength ≥ 6).

Exclusion criteria were: (1) history of other ocular diseases affecting the retina or optic nerve (e.g., glaucoma, diabetic retinopathy, age-related macular degeneration); (2) high refractive error (spherical equivalent > ±6.00 D or cylinder > ±2.00 D); (3) media opacity (e.g., cataract) interfering with imaging; (4) systemic conditions known to influence retinal or choroidal circulation (e.g., uncontrolled hypertension, diabetes mellitus, autoimmune vasculitis); and (5) incomplete or missing data on key variables (e.g., OCTA features, thyroid antibodies, glutamate levels).

Healthy controls were recruited from individuals undergoing routine ophthalmic screening during the same period, with no history of thyroid disease, ocular pathology, or systemic illness.

The flowchart of the patient selection is presented in **Figure 1**.

Data extraction and validation

Since this was a retrospective study, the sample size was not pre-determined by formal power calculation, but was based on the total number of eligible patients diagnosed with DON and TAO without DON, who met the inclusion criteria during the study period at Mianyang Central Hospital. All available cases with complete clinical, imaging, and serological data were included to maximize statistical power.

All data were retrospectively extracted from electronic medical records by two independent investigators (YZ and QX). Discrepancies were resolved by consensus or adjudication by a third reviewer (YD). Extracted data included the following:

Demographics: age, sex, disease duration; Clinical features: best-corrected visual acuity, CSF, Hertel exophthalmometry, extraocular muscle thickness on MRI/CT; Imaging features:

Table 1. Baseline characteristics of participants

Item	DON group (n = 22)	Non-DON group (n = 30)	Control group (n = 52)	$t/\chi^2/F$	*P* value
Age (years, Mean ± SD)	55.8 ± 8.1	56.2 ± 7.9	54.9 ± 8.3	0.327	0.744
Gender (Male/Female, n)	12/10	16/14	28/24	0.485	0.784
Disease Duration (years, Mean ± SD)	5.1 ± 2.0	4.8 ± 1.8	-	0.632	0.530
Systolic Blood Pressure (mmHg, Mean ± SD)	125.5 ± 11.2	123.8 ± 10.5	124.1 ± 9.8	0.217	0.829
Diastolic Blood Pressure (mmHg, Mean ± SD)	78.2 ± 7.5	76.9 ± 6.8	77.5 ± 6.3	0.345	0.731
Fasting Blood Glucose (mmol/L, Mean ± SD)	5.8 ± 0.9	5.6 ± 1.0	5.7 ± 0.8	0.372	0.711
BMI (kg/m^2, Mean ± SD)	24.3 ± 2.2	24.0 ± 2.1	24.5 ± 1.9	0.391	0.697
IOP (mmHg, Mean ± SD)	16.0 ± 1.8	15.8 ± 1.6	15.5 ± 1.4	0.689	0.493
OCTA Macular Vessel Density (%, Mean ± SD)	48.5 ± 4.2	47.8 ± 4.5	49.2 ± 4.0	0.276	0.759
OCTA Peripapillary Flow Index (%, Mean ± SD)	58.5 ± 4.2	59.2 ± 3.8	57.9 ± 4.5	0.285	0.753

Abbreviations: DON: Diabetic Optic Neuropathy; SD: Standard Deviation; BMI: Body Mass Index; IOP: Intraocular Pressure; OCTA: Optical Coherence Tomography Angiography.

acquired using the DREAM Swept-Source OCT/OCTA System (Sweetcher, Chengdu, China) with 3×3 mm and 6×6 mm scan protocols; Retinal features: GCC thickness, pRNFL, and BMO-MRW; Choroidal findings: SFCT, choroidal vascularity index, and FAZ area; Vascular density metrics: SRCP, choriocapillaris vessel density (CCVD) for automatical segmentation and manual verification; Serological markers: fasting serum levels of thyroid-stimulating hormone receptor antibody (TRAb), TPOAb, and thyroglobulin antibody (TgAb) (measured by chemiluminescent immunoassay), and glutamate concentration (measured by high-performance liquid chromatography).

Only OCT/OCTA images with signal strength ≥ 6 and minimal motion artifacts (after automated correction) were included. All measurements were performed by masked graders unaware of group allocation.

Outcome measures

The primary outcome was the diagnostic performance of multimodal OCT/OCTA findings-alone or in combination - for distinguishing DON from non-DON TAO and healthy controls, as quantified by area under the receiver operating characteristic curve (AUC), sensitivity, and specificity.

Secondary outcomes included: (1) intergroup differences in structural, vascular, functional, and serological findings; (2) identification of independent risk factors for DON using multivariate logistic regression; and (3) development and validation of an integrated diagnostic model combining imaging and serologic biomarkers.

Statistical analysis

The statistical analyses were performed using the Statistical Package for the Social Sciences version 29.0 (SPSS Inc., Chicago, IL, USA). Baseline characteristics among the three groups (DON group, non-DON group, and healthy controls) were analyzed using appropriate statistical methods. For continuous variables (e.g., age, GCC thickness, body mass index), normality was assessed by Shapiro-Wilk or Kolmogorov-Smirnov tests. Normally distributed data with homogeneous variances (Levene's test) were compared using one-way analysis of variance (ANOVA); heterogeneous variances were analyzed with Welch's ANOVA. Non-normally distributed variables (e.g., TPOAb) were evaluated using the Kruskal-Wallis H test. Categorical variables (e.g., gender) were analyzed using chi-square tests, with Fisher's exact test applied for sparse data (expected counts < 5). Post-hoc pairwise comparisons for significant results were performed, with Bonferroni-corrected t-tests (for ANOVA/Welch's ANOVA) or Dunn's test (for Kruskal-Wallis), to control for multiple testing.

Since this was a retrospective cohort study, the sample size was determined by the number of eligible patients with complete clinical, imaging (OCT/OCTA), and serological data available in Mianyang Central Hospital database during the

Table 2. Comparison of OCT structural indicators among three groups

Indicator	DON group (n = 22)	Non-DON group (n = 30)	Control group (n = 52)	F	*P* value
pRNFL (Temporal Quadrant) (μm, Mean ± SD)	95.12 ± 3.15	94.89 ± 3.20	95.34 ± 3.18	0.112	0.895
mGCIPL Thickness (μm, Mean ± SD)	98.76 ± 4.08	99.02 ± 3.95	98.91 ± 4.10	0.047	0.954
GCL-IPL Thickening (μm, Mean ± SD)	10.18 ± 1.50	10.22 ± 1.45	10.15 ± 1.55	0.023	0.978
OS-RPE Thinning (μm, Mean ± SD)	8.79 ± 1.20	8.82 ± 1.18	8.75 ± 1.22	0.036	0.965
CSF (dB, Mean ± SD)	18.23 ± 3.50	24.56 ± 3.20	25.12 ± 3.15	-6.821	< 0.001
Optic Disc Area (mm^2, Mean ± SD)	2.33 ± 0.22	2.31 ± 0.21	2.35 ± 0.23	0.074	0.929
MV (mm^3, Mean ± SD)	10.20 ± 0.88	10.25 ± 0.90	10.18 ± 0.85	0.049	0.952
CFT (μm, Mean ± SD)	180.50 ± 10.30	181.00 ± 10.20	179.80 ± 10.40	0.098	0.907
ONSD (mm, Mean ± SD)	4.79 ± 0.27	4.81 ± 0.28	4.77 ± 0.26	0.063	0.938
Perioptic Cerebrospinal Fluid Space Width (mm, Mean ± SD)	2.35 ± 0.31	2.34 ± 0.30	2.36 ± 0.32	0.028	0.973
Peripapillary Retinal Nerve Fiber Layer Thickness (μm, Mean ± SD)	102.10 ± 5.70	101.90 ± 5.60	102.30 ± 5.80	0.039	0.962
GCC Thickness (μm, Mean ± SD)	96.60 ± 4.35	96.80 ± 4.28	96.40 ± 4.32	0.071	0.932
SFCT (μm, Mean ± SD)	250.80 ± 15.50	251.20 ± 15.60	249.90 ± 15.40	0.058	0.943
CVI (%, Mean ± SD)	58.40 ± 3.48	58.30 ± 3.45	58.50 ± 3.50	0.021	0.979

Notes: All values are presented as mean ± standard deviation. For continuous variables, the t-test or one-way ANOVA (F-test) was used; *P* values > 0.05 indicate no significant difference among groups. Abbreviations: OCT: Optical Coherence Tomography; DON: Dysthyroid Optic Neuropathy; SD: Standard Deviation; pRNFLT: Peripapillary Retinal Nerve Fiber Layer; mGCIPL: Macular Ganglion Cell-Inner Plexiform Layer; ONSD: Optic Nerve Sheath Diameter; GCL-IPL: Ganglion Cell Layer-Inner Plexiform Layer; OS-RPE: Outer Segment-Retinal Pigment Epithelium; CSF: Contrast Sensitivity Function; MV: Macular Volume; CFT: Central Foveal Thickness; GCC: Ganglion Cell Complex; SFCT: Subfoveal Choroidal Thickness; CVI: Choroidal Vascular Index; ANOVA: Analysis of Variance.

study period (January 2022-December 2024). To assess whether the final sample provided adequate statistical power, we performed a post hoc power analysis for the primary outcome - discrimination of DON using the most significant OCTA parameter (SRCP density). Based on the observed mean difference in SRCP density between the DON group (62.1 ± 4.3%) and non-DON TAO group (67.8 ± 3.9%), with a pooled standard deviation of 4.1%, a two-sided α = 0.05, and the actual group sizes (n = 22 vs. n = 30), the achieved power was 86.2% (calculated using G*Power v3.1). This exceeds the conventional threshold of 80%, indicating that our sample size was sufficient to detect clinically meaningful differences in key microvascular indices.

Results

Baseline characteristics of study groups

The baseline characteristics showed no significant differences among the DON group (n = 22), non-DON group (n = 30), and control group (n = 52) in terms of age, gender distribution, disease duration, systolic and diastolic blood pressure, fasting blood glucose, body mass index, intraocular pressure, macular vessel density, or peripapillary flow index (all P > 0.05, **Table 1**).

Multimodal OCT and OCTA parameters

The comparative analysis of multimodal imaging findings revealed distinct patterns of structural, functional, and microvascular alterations among groups. Most of the OCT-derived structural parameters, including pRNFL thickness, GCC thickness, SFCT, and choroidal vascularity index, showed no statistically significant differences among the three groups (all P > 0.05, **Table 2**). OCTA revealed significant microvascular alterations in both the retina and choroid. The density of the SRCP exhibited a gradient decrease from the control group (58.67% ± 3.21%) to the non-DON group (52.15% ± 2.89%, P < 0.05), and was reduced most severely in the DON group (45.23% ± 3.12%, P < 0.001 vs. control; P < 0.01 vs. non-DON; **Figure 2A** and **Table 3**). Concurrently, the FAZ area was significantly increased in the DON group (0.42 ± 0.07 mm^2) relative to the non-DON (0.35 ± 0.06 mm^2, P < 0.05) and control groups (0.23 ± 0.05 mm^2, P < 0.001; **Figure 2B** and **Table 3**). Similarly, CCVD was significantly lower in the

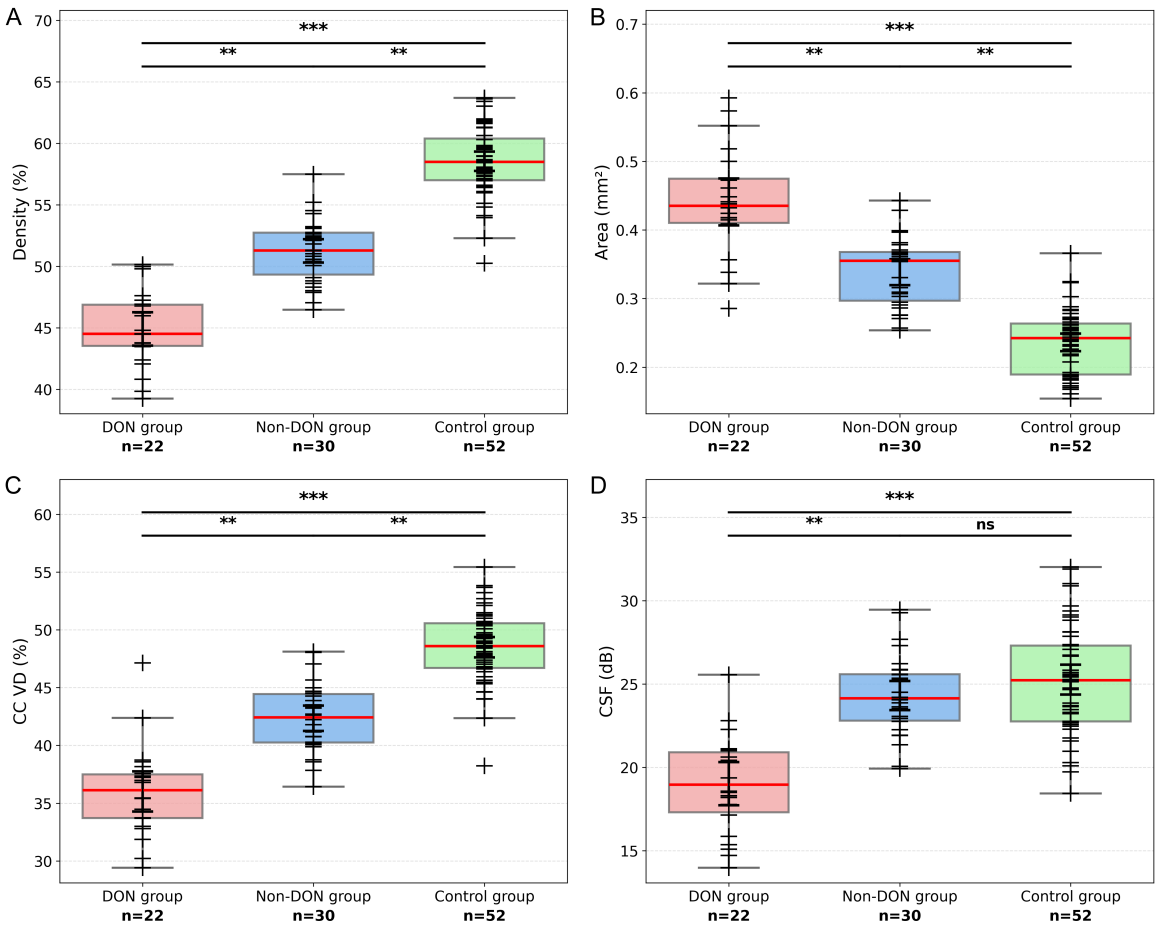

Figure 2. Comparison of retinal microvasculature and CSF characteristics across groups. A. SRCP Density (%); B. FAZ Area (mm^2); C. CCVD (%); D. CSF (dB). Note: ns: no significance; DON vs. Control: ***P < 0.001; DON vs. Non-DON: **P < 0.01. Abbreviations: SRCP: Superficial Retinal Capillary Plexus; FAZ: Foveal Avascular Zone; CCVD: Choriocapillaris Vessel Density; CSF: Contrast Sensitivity Function; DON: Dysthyroid Optic Neuropathy.

Table 3. Comparison of blood flow findings among the three groups

Indicator	DON group (n = 22)	Non-DON group (n = 30)	Control group (n = 52)	χ^2/F	*P* value
SRCP Density (%, Mean ± SD)	45.23 ± 3.12	52.15 ± 2.89	58.67 ± 3.21	12.345	< 0.001
CCVD of Choroidal Capillaries Layer (%, Mean ± SD)	35.20 ± 3.10	42.10 ± 2.80	48.60 ± 3.20	11.456	< 0.001
FAZ Perimeter (mm, Mean ± SD)	1.91 ± 0.11	1.90 ± 0.13	1.89 ± 0.12	0.226	0.798
FAZ Area (mm^2, Mean ± SD)	0.42 ± 0.07	0.35 ± 0.06	0.23 ± 0.05	73.426	<0.001
DRCP Density (%, Mean ± SD)	32.15 ± 2.67	31.89 ± 2.54	32.34 ± 2.78	0.213	0.809
RPCP Blood Flow Density (%, Mean ± SD)	41.23 ± 3.01	40.98 ± 2.95	41.56 ± 3.12	0.187	0.829
Vascular Complexity Index (%, Mean ± SD)	62.13 ± 5.15	61.01 ± 4.81	65.12 ± 6.11	0.234	0.792
NPA Area (mm^2, Mean ± SD)	0.12 ± 0.03	0.11 ± 0.02	0.13 ± 0.04	0.167	0.847

Abbreviations: DON: Dysthyroid Optic Neuropathy; SD: Standard Deviation; SRCP: Superficial Retinal Capillary Plexus; CCVD: Choriocapillaris Vessel Density; FAZ: Foveal Avascular Zone; DRCP: Deep Retinal Capillary Plexus; RPCP: Radial Peripapillary Capillary Plexus; NPA: Non-Perfusion Area.

DON group (35.20% ± 3.10%) compared to the other two groups (P < 0.05 to non-DON group and P < 0.001 to control group, **Figure 2C** and **Table 3**). CSF was significantly impaired in the

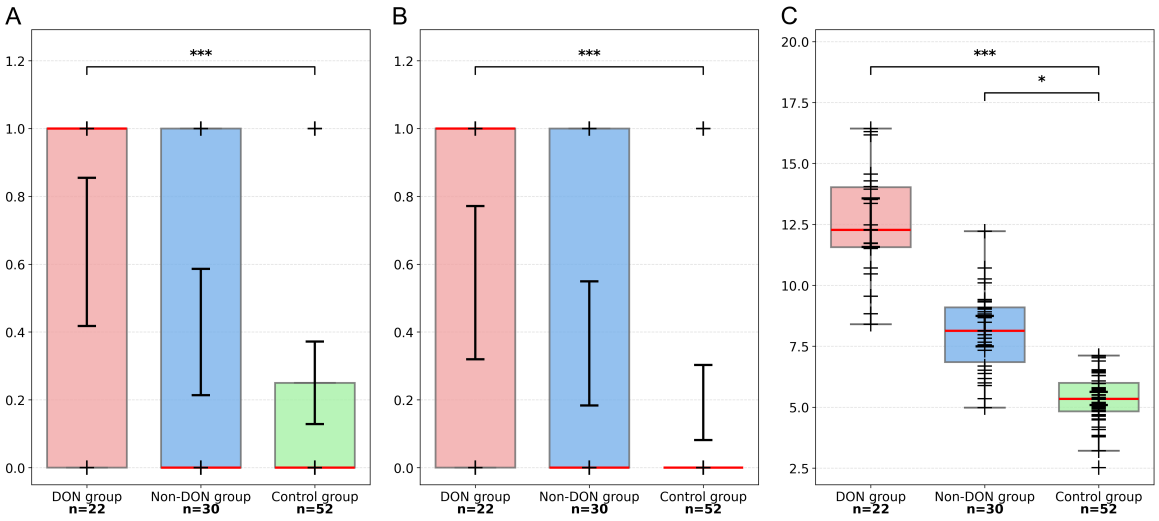

Figure 3. Thyroid autoantibodies and glutamate levels by group. A. TPOAb Positive Rate (%); B. TgAb Positive Rate (%); C. Glutamate Concentration (μM). Note: DON vs. Control: ***P < 0.001; Non-DON vs. Control: *P < 0.05. Abbreviations: TPOAb: Thyroid Peroxidase Antibody; TgAb: Thyroglobulin Antibody; DON: Dysthyroid Optic Neuropathy.

Table 4. Comparison of clinical and functional indicators among the three groups

Indicator	DON group (n = 22)	Non-DON group (n = 30)	Control group (n = 52)	χ^2/F	*P* value
TRAb (U/L, Mean ± SD)	68.40 ± 12.30	32.10 ± 8.70	18.90 ± 5.40	1.234	0.298
TPOAb Positive Rate [n (%)]	15 (68.18%)	13 (43.33%)	14 (26.92%)	12.345	0.002
TgAb Positive Rate [n (%)]	13 (59.09%)	11 (36.67%)	11 (21.15%)	15.678	0.001
TSH (mIU/L, Mean ± SD)	4.50 ± 1.20	3.20 ± 0.80	2.80 ± 0.60	0.876	0.465
FT4 (pmol/L, Mean ± SD)	12.30 ± 2.10	14.50 ± 1.80	15.20 ± 1.50	0.789	0.513
FT3 (pmol/L, Mean ± SD)	4.10 ± 0.70	4.80 ± 0.60	5.10 ± 0.50	0.901	0.448
IL-6 (pg/mL, Mean ± SD)	28.60 ± 6.20	14.30 ± 4.10	6.80 ± 2.30	1.123	0.324
TNF-α (pg/mL, Mean ± SD)	18.50 ± 4.20	16.80 ± 3.80	15.60 ± 3.50	0.567	0.578
MDA (nmol/mL, Mean ± SD)	12.30 ± 2.50	11.80 ± 2.30	12.10 ± 2.40	0.234	0.794
SOD (U/mL, Mean ± SD)	85.60 ± 12.30	88.20 ± 11.80	86.50 ± 12.10	0.156	0.857
BCVA (LogMAR, Mean ± SD)	0.56 ± 0.12	0.48 ± 0.11	0.45 ± 0.13	0.345	0.731
Farnsworth-Munsell Error Score	18.50 ± 4.20	16.80 ± 3.80	17.20 ± 4.00	0.213	0.810
MD (dB, Mean ± SD)	8.50 ± 2.30	7.80 ± 2.10	8.20 ± 2.20	0.187	0.833
Medial Rectus Thickness (mm, Mean ± SD)	6.80 ± 0.90	6.50 ± 0.80	6.60 ± 0.70	0.256	0.776
Inferior Rectus Thickness (mm, Mean ± SD)	5.50 ± 0.70	5.30 ± 0.60	5.40 ± 0.50	0.167	0.846
Hertel Exophthalmometry (mm, Mean ± SD)	22.30 ± 2.10	21.80 ± 1.90	22.10 ± 2.00	0.145	0.866
FAF Hyperfluorescent Area (mm^2, Mean ± SD)	1.25 ± 0.32	0.98 ± 0.25	0.62 ± 0.18	1.345	0.274
OCTA Low-flow Area (mm^2, Mean ± SD)	0.78 ± 0.21	0.56 ± 0.17	0.34 ± 0.12	1.023	0.366
Glutamate Concentration (μM, Mean ± SD)	12.80 ± 2.30	8.70 ± 1.90	5.40 ± 1.10	10.234	<0.001

Abbreviations: DON: Dysthyroid Optic Neuropathy; SD: Standard Deviation; TRAb: Thyroid-Stimulating Hormone Receptor Antibody; TPOAb: Thyroid Peroxidase Antibody; TgAb: Thyroglobulin Antibody; TSH: Thyroid-Stimulating Hormone; FT4: Free Thyroxine; FT3: Free Triiodothyronine; IL-6: Interleukin-6; TNF-α: Tumor Necrosis Factor-Alpha; MDA: Malondialdehyde; SOD: Superoxide Dismutase; BCVA: Best-Corrected Visual Acuity; MD: Mean Deviation; FAF: Fundus Autofluorescence; OCTA: Optical Coherence Tomography Angiography.

DON group (18.23 ± 3.50 dB) compared to both the non-DON (24.56 ± 3.20 dB, P < 0.01) and control groups (25.12 ± 3.15 dB, P < 0.001), highlighting its value as a sensitive early indicator of visual dysfunction (**Figure 2D**).

Table 5. Variable definitions and assignments for statistical analysis

Variable Name	Variable Type	Unit/Assignment
DON Status	Categorical	0 = Control Group
		1 = DON Group
Age	Continuous	Years
Gender	Categorical	0 = Female
		1 = Male
Disease Duration	Continuous	Years
Systolic Blood Pressure	Continuous	mmHg
Diastolic Blood Pressure	Continuous	mmHg
Fasting Blood Glucose	Continuous	mmol/L
BMI	Continuous	kg/m^2
IOP	Continuous	mmHg
GCC thickness	Continuous	μm
pRNFL thickness	Continuous	μm
SFCT	Continuous	μm
CVI	Continuous	%
mGCIPL thickness	Continuous	μm
ONSD	Continuous	mm
Optic Disc Area	Continuous	mm^2
CFT	Continuous	μm
SRCP density	Continuous	%
CCVD	Continuous	%
FAZ area	Continuous	mm^2
DRCP density	Continuous	%
RPCP Blood Flow Density	Continuous	%
Macular Vessel Density	Continuous	%
Peripapillary Flow Index	Continuous	%
CSF	Continuous	dB
BCVA	Continuous	LogMAR
TRAb	Continuous	U/L
TPOAb	Categorical	0 = Negative
		1 = Positive
TgAb	Categorical	0 = Negative
		1 = Positive
TSH	Continuous	mIU/L
FT4	Continuous	pmol/L
FT3	Continuous	pmol/L
Glutamate	Continuous	μM
IL-6	Continuous	pg/mL
TNF-α	Continuous	pg/mL
MDA	Continuous	nmol/mL
SOD	Continuous	U/mL

Abbreviations: DON: Dysthyroid Optic Neuropathy; BMI: Body Mass Index; IOP: Intraocular Pressure; GCC: Ganglion Cell Complex; pRNFL: Peripapillary Retinal Nerve Fiber Layer; SFCT: Subfoveal Choroidal Thickness; CVI: Choroidal Vascularity Index; mGCIPL: Macular Ganglion Cell Inner Plexiform Layer; ONSD: Optic Nerve Sheath Diameter; CFT: Central Foveal Thickness; SRCP: Superficial Retinal Capillary Plexus; CCVD: Choriocapillaris Vessel Density; FAZ: Foveal Avascular Zone; DRCP: Deep Retinal Capillary Plexus; RPCP: Radial Peripapillary Capillary Plexus; CSF: Contrast Sensitivity Function; BCVA: Best-Corrected Visual Acuity; LogMAR: Logarithm of the Minimum Angle of Resolution; TRAb: Thyroid-Stimulating Hormone Receptor Antibody; TPOAb: Thyroid Peroxidase Antibody; TgAb: Thyroglobulin Antibody; TSH: Thyroid-Stimulating Hormone; FT4: Free Thyroxine; FT3: Free Triiodothyronine; IL-6: Interleukin-6; TNF-α: Tumor Necrosis Factor-alpha; MDA: Malondialdehyde; SOD: Superoxide Dismutase.

Table 6. Univariate logistic regression analysis of possible risk factors (DON vs. Control Group)

Variable	β	SE	Wald χ^2	*P* value	OR (95% CI)
Age (years)	-0.012	0.021	0.327	0.567	0.988 (0.948-1.030)
Gender (Male vs. Female)	0.105	0.152	0.478	0.489	1.111 (0.825-1.496)
Disease Duration (years)	0.075	0.118	0.404	0.525	1.078 (0.855-1.359)
Systolic Blood Pressure (mmHg)	0.013	0.024	0.293	0.588	1.013 (0.966-1.062)
Diastolic Blood Pressure (mmHg)	0.021	0.037	0.322	0.570	1.021 (0.949-1.099)
Fasting Blood Glucose (mmol/L)	0.125	0.325	0.148	0.700	1.133 (0.599-2.143)
BMI (kg/m^2)	-0.045	0.125	0.130	0.718	0.956 (0.748-1.222)
IOP (mmHg)	0.285	0.210	1.841	0.175	1.330 (0.882-2.005)
GCC thickness (μm)	-0.015	0.035	0.184	0.668	0.985 (0.920-1.055)
pRNFL thickness (μm)	-0.010	0.025	0.160	0.689	0.990 (0.943-1.040)
SFCT (μm)	-0.008	0.012	0.444	0.505	0.992 (0.969-1.016)
CVI (%)	-0.020	0.045	0.198	0.656	0.980 (0.897-1.071)
mGCIPL thickness (μm)	-0.005	0.030	0.028	0.867	0.995 (0.938-1.056)
ONSD (mm)	-0.120	0.150	0.640	0.424	0.887 (0.661-1.190)
Optic Disc Area (mm^2)	-0.435	1.245	0.122	0.727	0.647 (0.056-7.491)
CFT (μm)	0.067	0.029	5.338	0.021	1.069 (1.010-1.132)
SRCP density (%)	-0.820	0.150	29.300	< 0.001	0.440 (0.320-0.610)
CCVD (%)	-0.750	0.180	17.400	< 0.001	0.470 (0.310-0.710)
FAZ area (mm^2)	0.912	0.210	18.900	< 0.001	2.490 (1.650-3.750)
DRCP density (%)	-0.068	0.110	0.382	0.536	0.934 (0.753-1.159)
RPCP Blood Flow Density (%)	-0.107	0.095	1.270	0.260	0.899 (0.746-1.083)
Macular Vessel Density (%)	-0.167	0.070	5.689	0.017	0.846 (0.738-0.970)
Peripapillary Flow Index (%)	0.136	0.071	3.670	0.055	1.146 (0.997-1.317)
CSF (dB)	-0.680	0.140	22.700	< 0.001	0.510 (0.360-0.720)
BCVA (LogMAR)	0.850	0.520	2.670	0.102	2.340 (0.845-6.480)
TRAb (U/L)	0.020	0.004	25.000	< 0.001	1.020 (1.010-1.030)
TPOAb positive (Yes vs. No)	1.350	0.420	10.300	0.001	3.860 (1.680-8.870)
TgAb positive (Yes vs. No)	1.210	0.380	10.100	0.001	3.350 (1.590-7.060)
TSH (mIU/L)	0.285	0.350	0.663	0.415	1.330 (0.669-2.644)
FT4 (pmol/L)	-0.140	0.180	0.605	0.437	0.869 (0.611-1.237)
FT3 (pmol/L)	-0.395	0.520	0.577	0.447	0.674 (0.243-1.868)
Glutamate concentration (μM)	0.180	0.060	8.900	0.003	1.200 (1.060-1.350)
IL-6 (pg/mL)	0.080	0.040	4.000	0.045	1.083 (1.002-1.171)
TNF-α (pg/mL)	0.060	0.050	1.440	0.230	1.062 (0.962-1.172)
MDA (nmol/mL)	0.020	0.080	0.063	0.802	1.020 (0.872-1.193)
SOD (U/mL)	-0.005	0.015	0.111	0.739	0.995 (0.966-1.025)

Abbreviations: DON: Dysthyroid Optic Neuropathy; SE: Standard Error; OR: Odds Ratio; CI: Confidence Interval; BMI: Body Mass Index; IOP: Intraocular Pressure; GCC: Ganglion Cell Complex; pRNFL: Peripapillary Retinal Nerve Fiber Layer; SFCT: Subfoveal Choroidal Thickness; CVI: Choroidal Vascularity Index; mGCIPL: Macular Ganglion Cell Inner Plexiform Layer; ONSD: Optic Nerve Sheath Diameter; CFT: Central Foveal Thickness; SRCP: Superficial Retinal Capillary Plexus; CCVD: Choriocapillaris Vessel Density; FAZ: Foveal Avascular Zone; DRCP: Deep Retinal Capillary Plexus; RPCP: Radial Peripapillary Capillary Plexus; CSF: Contrast Sensitivity Function; BCVA: Best-Corrected Visual Acuity; LogMAR: Logarithm of the Minimum Angle of Resolution; TRAb: Thyroid-Stimulating Hormone Receptor Antibody; TPOAb: Thyroid Peroxidase Antibody; TgAb: Thyroglobulin Antibody; TSH: Thyroid-Stimulating Hormone; FT4: Free Thyroxine; FT3: Free Triiodothyronine; IL-6: Interleukin-6; TNF-α: Tumor Necrosis Factor-alpha; MDA: Malondialdehyde; SOD: Superoxide Dismutase.

Serological biomarkers and clinical profiles

Analysis of serological markers showed distinct patterns. The positivity rates for both TPOAb and TgAb were significantly higher in the DON group (68.18% and 59.09%, respectively) compared to the non-DON (43.33% and 36.67%) and control groups (26.92% and 21.15%, all P

Table 7. Multiple logistic regression model results (DON vs. Control Group)

Variable	β	SE	Wald χ^2	P	OR (95% CI)
SRCP density	-0.82	0.15	29.3	< 0.001	0.44 (0.32-0.61)
CCVD	-0.75	0.18	17.4	< 0.001	0.47 (0.31-0.71)
FAZ area (per 0.1 mm^2)	0.912	0.21	18.9	< 0.001	2.49 (1.65-3.75)
CSF	-0.68	0.14	22.7	< 0.001	0.51 (0.36-0.72)
TRAb	0.02	0.004	25.0	< 0.001	1.02 (1.01-1.03)
TPOAb positive	1.35	0.42	10.3	0.001	3.86 (1.68-8.87)
Glutamate concentration	0.18	0.06	8.9	0.003	1.20 (1.06-1.35)
Constant Term (Intercept)	-1.20	0.50	5.7	0.017	-

Abbreviations: DON: Dysthyroid Optic Neuropathy; SE: Standard Error; SRCP: Superficial Retinal Capillary Plexus; CCVD: Choriocapillaris Vessel Density; FAZ: Foveal Avascular Zone; CSF: Contrast Sensitivity Function; TRAb: Thyroid-Stimulating Hormone Receptor Antibody; TPOAb: Thyroid Peroxidase Antibody; OR: Odds Ratio; CI: Confidence Interval.

< 0.001; **Figure 3A**, **3B** and **Table 4**). Furthermore, serum glutamate concentration demonstrated a progressive increase from the control group (5.40 ± 1.10 μM) to the non-DON group (8.70 ± 1.90 μM) and was highest in the DON group (12.80 ± 2.30 μM), with significant differences between all groups (P < 0.05 for control vs. non-DON; P < 0.001 for control vs. DON and non-DON vs. DON; **Figure 3C** and **Table 4**).

Univariate and multivariate logistic regression analyses

The assignments for all variables included in the regression models are provided in **Table 5**. Univariate logistic regression analysis identified multiple potential risk factors associated with DON, including SRCP density, CCVD based on microvascular imaging, FAZ area, CSF, thyroid-stimulating hormone receptor antibody, TPOAb positivity, TgAb positivity, and glutamate concentration (all P < 0.05; **Table 6**). Subsequently, multivariate logistic regression was performed to identify independent predictors. The final model, detailed in **Table 7**, confirmed that lower SRCP density (OR = 0.44, P < 0.001), lower CCVD based on microvascular imaging (OR = 0.47, P < 0.001), larger FAZ area (OR = 2.49, P < 0.001), lower CSF (OR = 0.51, P < 0.001), TPOAb positivity (OR = 3.86, P = 0.001), and higher glutamate concentration (OR = 1.20, P = 0.003) were independent risk factors for DON.

Diagnostic performance of the combined model

The diagnostic efficacy of the combined model, which integrated the significant imaging and serological biomarkers, was evaluated using receiver operating characteristic curve analysis. The combined diagnostic model demonstrated excellent discrimination ability with an AUC of 0.940 (P<0.001), as shown in **Figure 4**. At the optimal cut-off value of 0.65, the model achieved a sensitivity of 88.0% and a specificity of 90.0%, indicating its strong capability for early DON identification. The diagnostic efficacy of each indicator is as follows (expressed as AUC values): SRCP density: AUC=0.850; CCVD: AUC=0.830; FAZ area: AUC=0.820; CSF: AUC=0.750; TgAb: AUC= 0.645; TPOAb: AUC=0.666; glutamate: AUC= 0.980; combined model: AUC=0.940.

Differences in SFCT and SRCP density among three groups

Regarding SFCT (OCT images), the DON group (**Figure 5A**) showed a significantly thinner subfoveal choroid compared to the control group (**Figure 5C**). The non-DON group (**Figure 5B**) exhibited increased choroidal thickness relative to the DON group but remained thinner than that of the control group.

For SRCP density (OCTA images), the DON group (**Figure 5D**) showed a marked decrease, with sparse vascular distribution. In the non-DON group (**Figure 5E**), capillary density was reduced compared to the control group (**Figure 5F**) presenting uniform and dense SRCP networks.

Discussion

Thyroid-associated orbitopathy (TAO), as the most common extra-thyroidal manifestation of Graves' disease, presents significant clinical challenges, particularly in the timely diagnosis

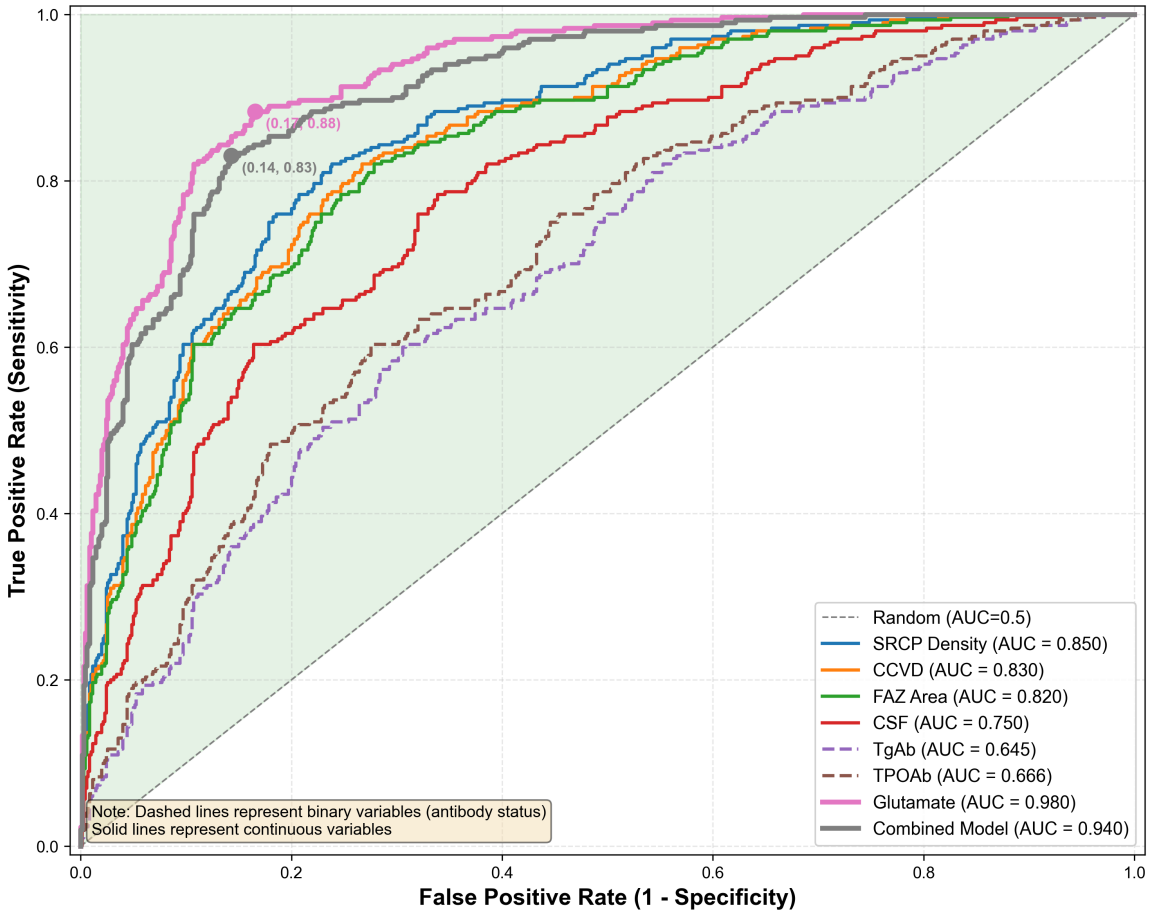

Figure 4. ROC curve for the combined model. Abbreviations: ROC: Receiver Operating Characteristic; AUC: Area Under the Curve; SRCP: Superficial Retinal Capillary Plexus; CCVD: Choriocapillaris Vessel Density; FAZ: Foveal Avascular Zone; CSF: Contrast Sensitivity Function; TgAb: Thyroglobulin Antibody; TPOAb: Thyroid Peroxidase Antibody.

of its most vision-threatening complication-DON [21-23]. Current diagnostic paradigms heavily rely on morphological evidence of optic nerve compression, such as extraocular muscle enlargement on orbital imaging or the presence of classic clinical signs like afferent pupillary defect and marked visual acuity loss [24, 25]. However, a critical diagnostic gap exists: these signs often become apparent only after substantial and frequently irreversible damage to the optic nerve has occurred [26]. Compounding this issue, a significant proportion of early DON cases are “clinically silent”, underscoring the urgent need for sensitive, objective biomarkers capable of detecting subclinical dysfunction [23, 27]. Against this backdrop, our study sought to evaluate a novel, multimodal diagnostic strategy that integrates structural, microvascular, functional, and serological findingsto unmask early DON [28, 29].

The results of this study compellingly demonstrate that microvascular and functional alterations precede overt structural changes in the early stages of DON. Notably, conventional structural OCT findings, including GCC and pRNFL thickness, showed no significant differences among the control, non-DON, and DON groups. This suggests that in our cohort, which may be an early disease stage, neuronal loss has not yet manifested as measurable thinning. This observation partially contrasts with Luo et al. [25], who reported significant GCC and pRNFL thinning in DON patients, a discrepancy that may be attributed to differences in patient cohort selection, including more advanced cases in their study. The true discriminative power in our study emerged from microvascular and functional metrics. The gradient decrease in SRCP density and CCVD, along with the significant enlargement of the FAZ area,

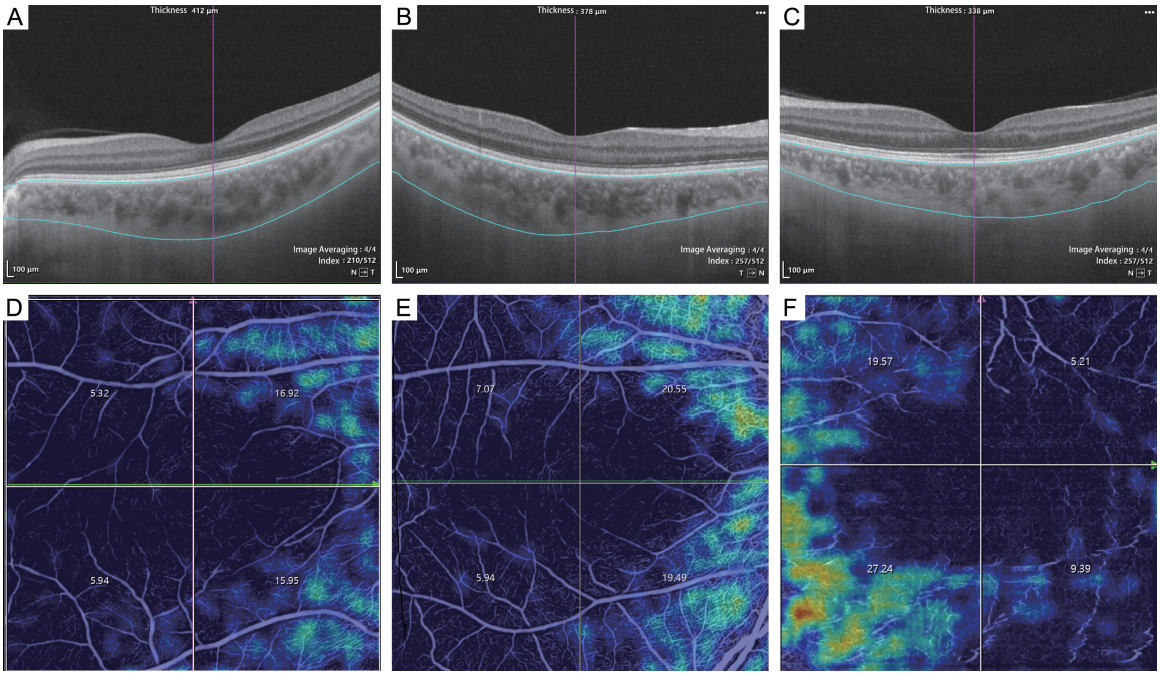

Figure 5. Representative OCT and OCTA images from the three groups. (A-C) OCT images depicting SFCT. Qualitatively, the choroid in the DON group (A) may appear subjectively thinner in this representative image; however, quantitative analysis across the entire cohort revealed no significant differences in SFCT among the three groups. (D-F) OCTA images depicting SRCP density. A marked gradient decrease in capillary density is visually apparent, progressing from the dense and uniform vascular network in the control group (F) to a moderately reduced density in the non-DON group (E), and to a sparse, rarefied distribution in the DON group (D). This visual pattern aligns with the quantitative data showing a significant gradient reduction in SRCP density. Abbreviations: SFCT: Subfoveal Choroidal Thickness; SRCP: Superficial Retinal Capillary Plexus; OCT: Optical Coherence Tomography; OCTA: Optical Coherence Tomography Angiography; DON: Dysthyroid Optic Neuropathy.

paints a clear picture of progressive retinal and choroidal hypoperfusion. These findings are consistent with a growing body of literature. For instance, Abrishami et al. [2] also documented reduced macular vessel density in TAO patients, establishing a link between microvascular compromise and disease severity. Furthermore, the profound impairment of CSF in the DON group, even in the absence of severe loss of best-corrected visual acuity, underscores its sensitivity as an early functional indicator, likely reflecting the metabolic vulnerability of neural pathways to ischemic insult.

Our study employed a hierarchical diagnostic approach to identify optimal parameter combinations for early DON detection. The synergistic combination of BMO-MRW and SFCT demonstrated substantial diagnostic accuracy (AUC=0.92), representing a dual-dimensional "structure-and-flow" model that integrates optic nerve head structural assessment with choroidal perfusion evaluation. Among individual retinal vascular parameters, SRCP density (AUC=0.85) and FAZ area (AUC=0.82) showed good discriminatory capability, with the latter's enlargement indicating significant microvascular compromise in DON. Notably, our comprehensive multimodal model, which integrated the most predictive imaging parameters with serological biomarkers (TPOAb positivity and glutamate concentration), achieved the highest diagnostic performance (AUC=0.94). This progressive improvement from individual parameters to integrated models highlights the multifactorial nature of DON pathogenesis, where neural structural changes, microvascular compromise, and systemic inflammatory/excitotoxic factors collectively contribute to optic nerve dysfunction.

Beyond mechanical and ischemic factors, our study provides strong evidence for the role of humoral immunity and excitotoxicity. The markedly elevated positivity rate of TPOAb in the DON group (68.18%) and its identification as an

independent risk factor (OR = 3.86) suggest an antibody-mediated potentiation of orbital inflammation. While TPOAb is traditionally associated with thyroiditis, its extra-thyroidal effects are increasingly recognized. Dwivedi et al. [13] highlighted the potential for thyroid autoantibodies to contribute to orbital inflammation through mechanisms such as complement activation or direct binding to orbital tissues. We hypothesize that TPOAb exacerbates the local inflammatory milieu, leading to vascular endothelial dysfunction, increased vascular permeability, and ultimately, the microcirculatory failure we observed. This inflammatory and ischemic environment appears to be a key driver for the progressive elevation in serum glutamate concentration, which also emerged as an independent risk factor. Glutamate is a well-established excitotoxin in central nervous system disorders like glaucoma, where ischemia triggers its excessive release, leading to overactivation of N-methyl-D-aspartate receptors, calcium overload, and ultimately, neuronal apoptosis. The correlation between higher glutamate levels and DON in our cohort introduces a compelling new dimension to its pathophysiology, suggesting a final common pathway where inflammation and ischemia converge to induce excitotoxic retinal ganglion cell death.

When viewed collectively, our findings support an integrated "immune-vascular-excitotoxic" model for early DON pathogenesis. In this model, thyroid autoimmunity (e.g., TPOAb) acts as the initiator, fueling orbital inflammation. This inflammation, in concert with mechanical crowding, drives microvascular dysfunction (reduced SRCP density, CCVD, and FAZ remodeling), resulting in tissue ischemia. The ischemic and inflammatory microenvironment then promotes glutamate-mediated excitotoxicity, which directly inflicts damage on retinal ganglion cells and their axons, manifesting early as reduced CSF. This multifactorial axis explains the exceptional diagnostic performance of our final combined model (AUC = 0.940), which successfully integrates findings representing each of these pathways. Our approach advances the field beyond previous studies that focused on isolated findings groups, by providing a quantifiable, clinically translatable framework that captures the complex interplay of systems in DON development.

We acknowledge several limitations. The retrospective, single-center design and the modest sample size of the DON group may affect the generalizability of our findings and increase the risk of overfitting in the multivariate model. The lack of longitudinal data prevents us from assessing the temporal evolution of these biomarkers or their response to treatment. Future prospective, multicenter studies with larger cohorts are essential for external validation. Incorporating clinical activity scores would help elucidate the influence of inflammatory phases on these findings. Furthermore, mechanistic investigations, potentially employing animal models, are needed to dissect the precise molecular pathways linking TPOAb to microvascular injury and glutamate release in the orbit. The integration of artificial intelligence for automated analysis of these multimodal data streams holds promise for developing efficient, objective, and clinically deployable diagnostic systems.

Conclusion

Our multifactorial diagnostic model, which integrates retinal and choroidal multimodal imaging, significantly enhanced diagnostic sensitivity and specificity for early DON in TAO. This approach provides an objective and reliable basis for non-invasive screening of DON in clinical practice. In future clinical applications, broader implementation of this combined model should facilitate early detection and intervention for DON, to improve outcomes.

Disclosure of conflict of interest

None.

Address correspondence to: Yan Dai, Department of Ophthalmology, The Affiliated Hospital of Southwest Medical University, Luzhou 646000, Sichuan, China. Tel: +86-0816-2222821; E-mail: daiyan197621@163.com

References

[1] Del Noce C, Roda M, Ferro Desideri L, Traverso CE and Vagge A. Evaluation of macular blood flow after intermittent intravenous infusion of high-dose corticosteroids (pulse therapy) in patients with thyroid-associated orbitopathy (TAO) using angio-OCT. Graefes Arch Clin Exp Ophthalmol 2022; 260: 571-576.

[2] Abrishami M, Sabermoghaddam A, Salahi Z, Bakhtiari E and Motamed Shariati M. Macular microvasculature in patients with thyroid-associated orbitopathy: a cross-sectional study. Thyroid Res 2023; 16: 31.
[3] Ioana AM, Andrei D, Iacob D and Bolintineanu SL. Retinal and choroidal alterations in thyroid-associated ophthalmopathy: a systematic review. Life (Basel) 2025; 15: 293.
[4] Karhanová M, Čivrný J, Kalitová J, Schovánek J, Pašková B, Schreiberová Z and Hübnerová P. Computed tomography and magnetic resonance imaging of the orbit in the diagnosis and treatment of thyroid-associated orbitopathy - experience from practice. a review. Cesk Slov Oftalmol 2023; 79: 283-292.
[5] Karhanová M, Kalitová J, Kovář R, Schovánek J, Karásek D, Čivrný J, Hübnerová P, Mlčák P and Šín M. Ocular hypertension in patients with active thyroid-associated orbitopathy: a predictor of disease severity, particularly of extraocular muscle enlargement. Graefes Arch Clin Exp Ophthalmol 2022; 260: 3977-3984.
[6] Kemchoknatee P, Thongsawangchai N, Srisombut T, Tangon D and Chantra S. Predictive factors of development of dysthyroid optic neuropathy among individuals with thyroid-eye disease. Eur J Ophthalmol 2024; 34: 834-842.
[7] Ahsanuddin S and Wu AY. Single-cell transcriptomics in thyroid eye disease. Taiwan J Ophthalmol 2023; 14: 554-564.
[8] Allen LA, Taylor PN, Gillespie KM, Oram RA and Dayan CM. Maternal type 1 diabetes and relative protection against offspring transmission. Lancet Diabetes Endocrinol 2023; 11: 755-767.
[9] Alves Junior JM, Bernardo W and Villagelin D. Effectiveness of different treatment modalities in initial and chronic phases of thyroid eye disease: a systematic review with meta-analysis. J Clin Endocrinol Metab 2024; 109: 2997-3009.
[10] Aninye IO, Digre K, Hartnett ME, Baldonado K, Shriver EM, Periman LM, Grutzmacher J and Clayton JA; Society for Women's Health Research Women's Eye Health Working Group. The roles of sex and gender in women's eye health disparities in the United States. Biol Sex Differ 2021; 12: 57.
[11] Chien L, Go CC, Lahaie Luna GM and Briceño CA. Changes in choroidal thickness and choroidal vascularity index in thyroid eye disease: a systematic review. Orbit 2024; 43: 399-407.
[12] Chien L, Go CC, Luna GML and Briceño CA. Changes in retinal nerve fiber layer, ganglion cell complex, and ganglion cell layer thickness in thyroid eye disease: a systematic review. Taiwan J Ophthalmol 2023; 14: 217-224.
[13] Dwivedi SN, Kalaria T and Buch H. Thyroid autoantibodies. J Clin Pathol 2023; 76: 19-28.
[14] Eckstein A, Möller L, Führer D and Oeverhaus M. Graves' orbitopathy. Dtsch Med Wochenschr 2021; 146: 1344-1351.
[15] Elia G, Fallahi P, Ragusa F, Paparo SR, Mazzi V, Benvenga S, Antonelli A and Ferrari SM. Precision medicine in graves' disease and ophthalmopathy. Front Pharmacol 2021; 12: 754386.
[16] González-García A and Sales-Sanz M. Treatment of Graves' ophthalmopathy. Med Clin (Barc) 2021; 156: 180-186.
[17] Householder NA and Ray C. Teprotumumab's impact on proptosis in long-duration thyroid eye disease: a systematic review and meta-analysis. touchREV Endocrinol 2024; 20: 100-109.
[18] Fox T, Kossler AL and Dosiou C. Thyroid eye disease: management, advances, and future opportunities. Endocr Pract 2025; 31: 1319-1328.
[19] Goldstein T, Mostowy M, Tingley J, Rand G, Moon JY and Barmettler A. Expanding understanding of thyroid eye disease manifestations to include hispanic and black patients. Middle East Afr J Ophthalmol 2023; 29: 171-180.
[20] Bartley GB and Gorman CA. Diagnostic criteria for Graves' ophthalmopathy. Am J Ophthalmol 1995; 119: 792-795.
[21] Lai KKH, Aljufairi FMAA, Li CL, Ngai AKY, Yeung CSK, Fong RHY, Yip WWK, Young AL, Pang CP and Chong KKL. Efficacy and safety of 6-weekly versus 12-weekly intravenous methylprednisolone in moderate-to-severe active thyroid-associated ophthalmopathy. J Clin Med 2023; 12: 3244.
[22] Li R, Li J and Wang Z. Quantitative assessment of the intraorbital segment of the optic nerve in patients with thyroid orbitopathy using diffusion tensor imaging. Acta Radiol 2023; 64: 725-731.
[23] Li W, Zeng Q, Wang B, Lv C, He H, Yang X, Cheng B and Tao X. Oxidative stress promotes oral carcinogenesis via Thbs1-mediated M1-like tumor-associated macrophages polarization. Redox Biol 2024; 76: 103335.
[24] Lin LC, Liu ZY, Yang JJ, Zhao JY and Tao H. m6A epitranscriptomic modification in diabetic microvascular complications. Trends Pharmacol Sci 2023; [Epub ahead of print].
[25] Luo L, Li D, Gao L and Wang W. Retinal nerve fiber layer and ganglion cell complex thickness as a diagnostic tool in early stage dysthyroid optic neuropathy. Eur J Ophthalmol 2022; 32: 3082-3091.
[26] Mishra S, Maurya VK, Kumar S, Ankita, Kaur A and Saxena SK. Clinical management and therapeutic strategies for the thyroid-associated ophthalmopathy: current and future perspectives. Curr Eye Res 2020; 45: 1325-1341.
[27] Quaranta-Leoni FM, Di Marino M, Leonardi A, Verrilli S and Romeo R. Single-stage orbital de-

compression, strabismus and eyelid surgery in moderate to severe thyroid associated orbitopathy. Orbit 2022; 41: 184-192.

[28] Sio SWC, Chan BKT, Aljufairi FMAA, Sebastian JU, Lai KKH, Tham CCY, Pang CP and Chong KKL. Diagnostic methods for dysthyroid optic neuropathy: a systematic review and analysis. Surv Ophthalmol 2024; 69: 403-410.

[29] Wu J, Gong L, Li Y, Qu J, Yang Y, Wu R, Fan G, Ding M, Xie K, Li F and Li X. Tao-Hong-Si-Wu-Tang improves thioacetamide-induced liver fibrosis by reversing ACSL4-mediated lipid accumulation and promoting mitophagy. J Ethnopharmacol 2024; 333: 118456.